

N74-19440

4. Combined Observations of Meteors by Image-Orthicon Television Camera and Multi-Station Radar

A. F. COOK, G. FORTI, R. E. McCROSKY,
A. POSEN, R. B. SOUTHWORTH, AND J. T. WILLIAMS
*Smithsonian Astrophysical Observatory
Cambridge, Massachusetts*

OBSERVATIONS FROM MULTIPLE SITES of a radar network and by television of 29 individual meteors from February 1969 through June 1970 are reported. The primary purpose of the program was to compare ionization with luminosity. Only 12 of the meteors did not appear to fragment over all the observed portion of their trajectories. From these 12, the following relation for the radar magnitude M_R to the panchromatic absolute magnitude M_p , in terms of velocity of the meteor V , was found:

$$M_R - M_p = +2.85 - 3.8(\log V - 6.41) \\ \pm 0.16 \pm 1.3$$

The double-signed quantities are standard deviations. The standard deviation for a single meteor is ± 0.5 . This result applies for meteors fainter than panchromatic absolute magnitude $+4.7$ and in the velocity range 14.7 to 36.0 km s^{-1} .

A very tentative fit to the data on the duration of long-enduring echoes versus visual absolute magnitude is made. The assumption that brighter meteors produce a higher ratio of ionization to light is required.

The exponential decay characteristic of the later parts of several of the light curves is pointed out as possible evidence of mutual coalescence of droplets into which the meteoroid has completely broken.

RADAR EQUIPMENT, OBSERVATIONS, AND REDUCTIONS

Radar

An eight-station multistatic phase-coherent pulsed Doppler radar system located in the area between Peoria and Springfield, Illinois, was used to observe meteors. The system had the following composition:

(a) A main site for the transmitter and a dual-channel receiver

(b) Five outlying sites arranged about the main site within 24 km, each equipped with a single-channel receiver

(c) Two remote sites about 34 and 47 km from the main site, each also equipped with a single-channel receiver

The system was able to collect phase-coherent meteor echoes from a volume in the upper atmosphere that is not sharply bounded but measures roughly $50 \text{ km} \times 50 \text{ km}$ horizontally and 20 km vertically over the range 80 to 100 km above mean sea level. The volume under radar patrol lies approximately above Decatur, Illinois.

When a meteor passed through this volume, echoes were received at the main site if the trail was tangent to a sphere centered at the main site. This sphere had a radius equal to the minimum range of the meteor from the main site; i.e., the meteor was observed via back scattering from the electrons of its trail. An echo was received at any

particular remote site if the trail was tangent to an ellipsoid with foci at the remote site (receiver) and the main site (transmitter).

At the main site, a nominal 4-MW peak power VHF transmitter was operated; the transmitter rarely ran at over 2 MW. The frequency employed was 40.92 MHz. The dual-channel receiver provided range, angle of arrival relative to a vertical reference plane, a Fresnel pattern, and radial velocity (Doppler information) on the back-scattered echoes received from a trail.

At each of the outlying and remote sites, a single-channel receiver provided range, a Fresnel pattern, and Doppler shift for forward-scattered echoes received from the trail.

The measurements were conveyed by microwave links to the main site, processed in a digitizer, and recorded by a multichannel digital tape recorder. All the data on the digitized tape were later processed at the Smithsonian Astrophysical Observatory's CDC 6400 computer in Cambridge, Massachusetts.

The computer program reads the tape (34 channels of information), processes the data to obtain positional information on the meteor trail and on its motion due to winds, and prints out the results.

Geographic Layout

Four of the five outlying stations are located approximately along a line with the main site bearing about 125° east of north in the order 1, 2, 3, 5, and 6, where site 3 is the main site. Site 4 is offset approximately perpendicularly from this line. The approximate spacing between sites is 12 km. Finally, the two remote sites, 7 and 8, are offset almost perpendicularly to the line 1, 2, 3, 5, and 6 at a distance of about 35 km so that stations 7, 6, and 8 also lie nearly in a straight line.

Rectangular coordinates x , y , and z are given in table 1 on axes east, north, and vertical from the main site, respectively; i.e., the system is an alt-azimuth system referred to the horizon and true north of the main site.

Simplified System Description

Figure 1 is a simplified block diagram of the radar, exhibiting station 3 near Havana, Illinois, and any one of the other stations. At sites 1 to 6,

TABLE 1.—Rectangular Coordinates of Radar Receiving Stations and Ranges from the Transmitter at Havana^a

Site number	x (km)	y (km)	z (km)	R_{03n} (km)
1	-19.89	+11.83	-0.01	23.14
2	-9.66	+8.15	+0.02	12.64
3	0.00	0.00	0.00	0.00
4	+5.04	+10.26	-0.01	11.43
5	+9.65	-6.31	+0.03	11.53
6	+22.10	-7.02	+0.01	23.19
7	+41.85	+22.03	-0.12	47.29
8	+0.67	-34.41	-0.06	34.42

^a The x axis is toward the east point, the y axis toward the north point, and the z axis toward the zenith as seen from the transmitter, and the origin is at the transmitter.

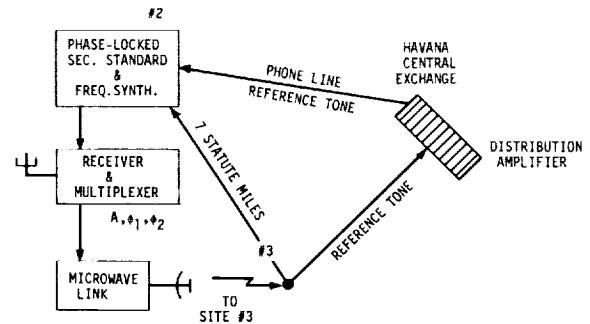


FIGURE 1.—General system layout.

trough antennas were directed toward azimuth 113° east of north. At sites 7 and 8, Yagi antennas were directed toward azimuths 139° and 94° east of north, respectively. The transmitter at site 3 (the main site) had a nominal peak power of 4 MW, which was never attained (2 MW being the usual power), and transmitted at 40.92 MHz (7.33 m). Both of the two troughs used for reception were also used for transmission.

The system at the main site produced the transmitted frequency, the mixer and reference frequencies for the receiver at the main site, and the 2.5-kHz reference frequency, sent by telephone line, for the outlying sites (1, 2, 4, 5, 6) and the remote sites (7, 8).

The transmitted pulse radiated from the transmission antenna at the main site was reflected by meteors (and aircraft), and these reflections were received at any or all of the sites. The echoes

received at the outlying and remote sites were transmitted back to the main site via microwave links.

At the main site, all the echoes were analyzed by echo-pattern recognizers. When an echo was accepted for recording, that echo was gated through gating circuits to the digitizer and a cathode-ray-tube film recorder. The main unit supplied the pulse-repetition frequency to the transmitter and range information and control to both the digitizers and the cathode-ray-tube film recorder.

Calibration of the receivers was carried out as follows: The antenna was disconnected from the receiver, and simulated echoes of known amplitude were sent to the receivers from the calibrator. Control signals for the calibrator were received from the main station via the microwave link in the form of switching tones and the pulse-repetition frequency. The tones were decoded by a tone receiver, which controlled the calibrator.

The receiver produced three outputs: The amplitude A pulse was proportional to the logarithm of the amplitude A_1 of the echo. It was sent to the main station via the microwave link on a 2.3-MHz subcarrier. Phase 1 (ϕ_1) and phase 2 (ϕ_2) pulses were proportional to $A_1 \cos \phi$ and $A_1 \sin \phi$, where ϕ is the phase of the echo relative to the transmitted phase. They were multiplexed in time and sent to the master station via the microwave link.

The receiver at the main site produced the same three outputs (A , ϕ_1 , ϕ_2), as well as ϕ_3 and ϕ_4 , the phase signals from the second trough of the double trough.

Reduction of Radar Data

Location of the Meteor and Measurement of Wind

Multiple Receiver System.—The epoch of the radar echo from the main site locates the meteor on a sphere about the main site of the observed range. The epoch of the echo from an outlying or remote site locates the meteor on an ellipsoid, with foci at the main site and the outlying or remote site, having the loop range (from the main site to the meteor, then to the remote site, and finally back to the main site) observed. The Fresnel patterns combined with the ranges yield

the velocity of the meteor. In favorable cases, the deceleration can be determined. If three stations have received echoes from a meteor and if the stations do not lie on a straight line, the intervals between the epochs of passage through the minimum loop range as determined from the Fresnel pattern determine the radiant of the meteor (a double solution occurs but with one direction below the horizon). From the radiant and range, it is, in principle, possible to locate the meteor on a circle or an ellipse on the appropriate sphere or ellipsoid at each epoch. Projection of these on a plane perpendicular to the radiant would then locate the trail. The projected circles and ellipses do not intersect at large enough angles for this procedure to work in practice.

Extra information is required and was obtained by using an interferometric arrangement at the main site and measuring the angle of arrival of the echo from a vertical plane. A cone is thus determined for each echo at the main site. Its intersection with the plane of the circle that is normal to the radiant and has a radius equal to the range will be two straight lines, one above and one below the horizon; we can reject the latter. This intersection at a right angle between the circle and the line locates the trail to an accuracy set primarily by the accuracy of measurement of the angle of arrival. In practice, the phase difference measured in the interferometer is uncertain by a whole number of waves, so that up to three solutions are possible. The solution that lies in the antenna beam and at a reasonable height above sea level is the one chosen.

Scattering Properties of the Meteoric Trail.—We assume that all the trails were underdense, i.e., that the radio wave was scattered by individual free electrons each of which oscillated as if no others were present. The minimum range point is the so-called specular reflection point.

This situation has been treated by many authors, but we shall rely here on McKinley (1961). Of the whole trail, the effective length that contributes to the scattering is $\sqrt{2R_0\lambda} \approx 1.5$ km in the back-scattering case (R_0 is the minimum range; λ , the wavelength). In the forward-scattering cases for the outlying and remote receivers, the lengths may be slightly different. Different stations received scattered signals from different parts of the trail.

Winds in the upper atmosphere displaced the specular reflection points, and physical processes altered the amplitude of the received echoes. Both these effects are small enough to be neglected in the initial approximation and are included later when the data are good enough to allow their measurement. Account was taken of diffusion and recombination.

Position of the Meteoric Trail.—The five outlying stations and the main site were located so as to permit approximate determinations of radiants and very rough determinations of meteor positions. If either of the two remote sites is involved in an observation along with any two of the main and outlying sites, then a rather good radiant and a fair determination of position can be expected. In all cases, an optical observation by the image-orthicon camera from Sidell, Illinois, greatly strengthens the determination. The present discussion is confined to the radar observations alone. Determination of trajectories, including optical observations, will be discussed further below. A least-squares fit is made if the meteor was observed at four or more receiving stations that do not all lie along a straight line.

Wind Measurements.—The received echo at each station conveys information concerning mainly the principal Fresnel zone, some 1.5 km in length. In general, each station observed a different portion of the trail. The spacing for the main site and the five outlying stations is typically up to 3.5 km in distance along the trail and up to 2.5 km in height. Larger spacings may occur for the two remote sites.

Measurements of phase at each station furnish a pseudoradial component of the wind velocity averaged over the first Fresnel zone. This measured component is directed along the bisector of the directions of the center of the principal Fresnel zone as seen from the main site and an outlying or remote site. This wind component is assumed to be horizontal, so that the pseudoradial horizontal wind needed to produce the observed pseudoradial wind is computed. It lies along the horizontal projection of the pseudoradial direction of measurement. The first derivative of the pseudoradial wind component with respect to distance along the trail is also found from the phase information and is transformed into a derivative

with respect to height of the pseudoradial horizontal wind.

If the meteor was observed at a remote site during the interval covered by observations from the main site and the outlying sites, a mean direction and fit for the pseudoradial horizontal wind can be found for the main site and outlying sites and interpolated to the epoch of the observation from the remote site. Combination with the pseudoradial horizontal wind from the remote site allows a determination of the horizontal wind at that point in the atmosphere.

Finally, the pseudoradial horizontal wind and its derivative with height are used to correct the determination of the meteor's radiant and position.

Phase-Coherent System

Figure 1 exhibits a block diagram of the main site near Havana, and one of the outlying or remote sites. The transmitter at the main site had a nominal power of 4 MW, which was never attained, and transmitted at 40.92 MHz (7.33 m).

The establishment of reference phase for the received signals imposed the following design requirements: The relative phase jitter between the transmitter and the local oscillators of the various superheterodyne receivers must not be larger than 10 percent of the minimum detectable Doppler shift. At a signal-to-noise ratio of 20 db and for a meteor duration of 0.05 s, the minimum detectable Doppler shift for the radiated waveform is 0.25 Hz (Grossi, 1963). Consequently, a relative stability of 5 parts in 10^{10} was needed.

This requirement was met by the following system: A single master oscillator at 1 MHz operated at the main site, from which, by frequency synthesis, the frequencies required for the transmitter and the local oscillators of the dual-channel receivers were obtained. Division down of the 1-MHz frequency to 2.5 kHz (400:1) yielded a reference signal for distribution by telephone line to the other seven sites. The telephone lines were not free from phase jitter. Accordingly, the phase of the reference tone arriving by telephone line at each station was compared to a local secondary standard (VCO). The output of this phase comparator was passed through an integrator with a 10-min time constant, thereby locking the phase of the local secondary standard to the 10-min average of the incoming reference tone.

This procedure effectively suppressed the phase jitter in the telephone lines.

Range measurements for the waveform employed at a signal-to-noise ratio of 20 db, a pulse width of 6 μsec , a pulse-repetition period of 1355 μsec , and target detectability lasting 0.05 s are, in principle, possible to a standard deviation of ± 10 m. The actual tolerable range error was taken to be ± 100 m for purposes of design. Actual performance on these meteors has been closer to a standard deviation of ± 1 km. These numbers apply to the half loop range and are to be doubled for total loop range.

Mathematical Outline of Radar Reductions

Wind-Phase Information

If a meteor perchance leaves a trail of electrons that is not underdense but resonant, the corresponding phase shift varies with time in a way not possible for winds; such cases can thus be eliminated at once.

We shall begin by considering the case of back scatter. We let the x axis lie along the trajectory of the meteor, the origin lie at the minimum range point, and the radar station lie on the negative y axis. The distance D from any point (x, y) to the radar station is

$$D = [(R+y)^2 + x^2]^{1/2} = (R^2 + 2Ry + x^2 + y^2)^{1/2}$$

and expansion by the binomial theorem followed by linearization in x^2 and y yields

$$D \cong R + y + \frac{x^2}{2R} \quad (1)$$

The phase ϕ is taken with respect to an element at the origin (which differs only by a constant from that of the transmitted wave):

$$\phi = \frac{4\pi(D-R)}{\lambda} \cong \frac{2\pi x^2}{\lambda R} + \frac{4\pi y}{\lambda} \quad (2)$$

Only the y component of the wind need be considered, and we expand this component in a Maclaurin series about the origin, retaining only the first two terms:

$$\dot{y} \cong -ax_w + ax$$

i.e., we have defined the radial component of the

wind in such a way that we can write

$$\dot{y} \cong a(x - x_w) \quad (3)$$

where x_w is now that point in x at which the radial component of the wind would vanish if we consider only the first two terms in the Maclaurin series.

We denote time by t and the epoch at which the meteor passes the origin by t_0 . Then the coordinates of the meteor, x_m, y_m , are

$$x_m = V(t - t_0) \quad y_m = 0 \quad (4)$$

The coordinate of any element of the ionized trail can then be found from its radial speed and the interval τ since it was generated by the meteoroid:

$$y = \dot{y}\tau = a(x - x_w) \left(t - t_0 - \frac{x}{V} \right) \quad (5)$$

$$y = - \left(\frac{a}{V} \right) \{ x^2 - [x_w + V(t - t_0)]x + x_w V(t - t_0) \}$$

The phase of the echo from an element at x is found by substitution of equation (5) into equation (2):

$$\begin{aligned} \phi = & \left(\frac{2\pi}{\lambda R} \right) \left(1 - \frac{2aR}{V} \right) \left\{ x + \frac{aR[t - t_0 + (x_w/V)]}{1 - (2aR/V)} \right\}^2 \\ & - 2\pi \left(\frac{a^2 R}{\lambda} \right) \left\{ \left[\frac{[t - t_0 + (x_w/V)]^2}{1 - (2aR/V)} \right] + 2x_w \frac{t - t_0}{aR} \right\} \end{aligned} \quad (6)$$

We introduce a dimensionless parameter α for the wind shear:

$$\alpha \equiv \frac{aR}{V} \quad (7)$$

so that we rewrite equation (6) as

$$\begin{aligned} \phi = & \left(\frac{2\pi}{\lambda R} \right) (1 - 2\alpha) \left\{ x + \frac{\alpha[x_w + V(t - t_0)]}{1 - 2\alpha} \right\}^2 \\ & - \left(\frac{2\pi}{\lambda R} \right) \alpha \left\{ \left[\frac{\alpha[x_w + V(t - t_0)]^2}{1 - 2\alpha} \right] + 2x_w V(t - t_0) \right\} \end{aligned} \quad (8)$$

The second term on the right-hand side of equation (8) is independent of x and, therefore, applies to the phase of the integrated echo. We denote this term, the phase variation due to the

wind, by the symbol Φ ,

$$\Phi \equiv - \left(\frac{2\pi}{\lambda R} \right) \alpha \left(\left\{ \frac{\alpha [x_w + V(t-t_0)]^2}{1-2\alpha} \right\} + 2x_w V(t-t_0) \right) \quad (9)$$

The first term on the right-hand side of equation (8) is best examined by comparison with the phase ϕ' at vanishing wind shear:

$$\phi' \equiv \left(\frac{2\pi}{\lambda R} \right) x'^2 \quad (10)$$

We see that

$$x' \equiv (1-2\alpha)^{1/2} \left\{ x + \frac{\alpha [x_w + V(t-t_0)]}{1-2\alpha} \right\} \quad (11)$$

Thus, the amplitude of the Fresnel pattern (see the derivation given by McKinley, 1961, pp. 186-198) appears as for a meteor of velocity V' that passes through minimum range at an epoch t'_0 , where

$$V' = V(1-\alpha)(1-2\alpha)^{-1/2} \quad (12)$$

$$t'_0 - t_0 = -\alpha x_w (1-\alpha)^{-1} V^{-1} \quad (13)$$

The Fresnel patterns yield V' and t'_0 , which we now wish to employ, by means of equation (9), in interpreting the phase variation due to the wind. Accordingly, we solve equations (12) and (13) for V and $t_0 - t'_0$ and substitute into equation (9) to find

$$\begin{aligned} \Phi - \Phi_0 &= - \frac{2\pi}{\lambda R} \left(\frac{\alpha}{1-\alpha} \right)^2 [V'(t-t'_0)]^2 \\ &\quad - \frac{4\pi}{\lambda R} \left[1 - \left(\frac{\alpha}{1-\alpha} \right)^2 \right] \frac{\alpha x_w}{(1-2\alpha)^{1/2}} V'(t-t'_0) \end{aligned} \quad (14)$$

where Φ_0 is the phase variation due to the winds at epoch t'_0 , the apparent epoch of minimum range. Equation (14) is then the expression for the change in phase since that epoch due to the winds. Evidently we can evaluate $[\alpha/(1-\alpha)]^2$ and $\alpha x_w/(1-2\alpha)^{1/2}$. From equations (12) and (13) it is apparent that we have

$$V = V' \left[1 - \left(\frac{\alpha}{1-\alpha} \right)^2 \right]^{1/2} \quad (15)$$

$$t_0 - t'_0 = \frac{\alpha x_w}{(1-2\alpha)^{1/2}} \frac{1}{V'} \quad (16)$$

From equation (12) or (15) we see that $\alpha \ll 1/2$

is required. Not only does accuracy become lost as α approaches $1/2$, but at $\alpha = 1/2$ the curvature of the trail equals that of the wavefront and we receive an echo simultaneously from all along its length. Near this condition we would receive an anomalously strong echo. In fact, from equation (15) it is apparent that the received amplitude should be rescaled by a factor

$$\left[1 - \left(\frac{\alpha}{1-\alpha} \right)^2 \right]^{1/2}$$

to allow for the altered lengths of the Fresnel zones. For α locally greater than $1/2$ and varying in the usual roughly sinusoidal way with height, we would receive multiple echoes and the meteor would not have been accepted for reduction.

The actual point of tangency between the radar wavefronts and the ionized column plainly lies at $x' = 0$, so from equation (11) we have

$$x_0 = - \frac{\alpha}{1-2\alpha} [x_w + V(t-t_0)] \quad (17)$$

$$y_0 = - \frac{1}{2R} \frac{\alpha^2}{1-2\alpha} [x_w + V(t-t_0)]^2 - \frac{\alpha x_w}{R} V(t-t_0) \quad (18)$$

where we have obtained y_0 by multiplying equation (9) by $\lambda/4\pi$. Elimination of time yields the parabola

$$y_0 = - \frac{1}{2} (1-2\alpha) \frac{x_0^2}{R} + (1-2\alpha) \frac{x_w}{R} x_0 + \alpha \frac{x_w^2}{R} \quad (19)$$

which is concave toward the station. It is evident that α must be quite small or our reflection would migrate to quite a different part of the trail from the minimum range point corresponding to the absence of wind.

Observations of the wind phase yield the quantities G and H' , defined as

$$G \equiv \left| \frac{\alpha}{1-\alpha} \right| \quad (20)$$

$$H' \equiv \left[1 - \left(\frac{\alpha}{1-\alpha} \right)^2 \right] \frac{\alpha x_w}{(1-2\alpha)^{1/2}} \quad (21)$$

There are two roots for α , from equation (20):

$$\alpha = \frac{G}{1+G} \quad - \quad \frac{G}{1-G} \quad (22)$$

and two corresponding roots for x_w , from equation (21):

$$H \equiv \frac{H'}{(1-G^2)^{1/2}} \quad x_w = \pm \frac{H}{G} \quad (23)$$

We recall the definition (7) to find, for the wind shear,

$$a = \frac{V}{R} \frac{G}{1+G} \quad - \frac{V}{R} \frac{G}{1-G} \quad (24)$$

The two expressions from equation (3) for the wind are

$$\dot{y} = \frac{V}{R} \frac{G}{1+G} \left(x - \frac{H}{G} \right) \quad - \frac{V}{R} \frac{G}{1-G} \left(x + \frac{H}{G} \right) \quad (25)$$

which are equal at

$$x = -H \quad \dot{y} = - \frac{V}{R} H \quad (26)$$

the point at which the meteor passed through minimum range on the trail distorted by the wind field. This measured radial component of the wind and the two alternative values for the shear (eq. (24)) of this component along the trail comprise all the information that we can obtain from phase measurement from one station. The corrected velocity becomes

$$V = V'(1-G^2)^{1/2} \quad (27)$$

and the corrected epoch of passing minimum range becomes

$$t_0 - t'_0 = (1-G^2)^{1/2} \frac{H}{V'} \quad (28)$$

both independent of the selected root for a in equation (24).

The case in which the transmitter and the receiver are at different sites is very similar to the foregoing. The essential difference is that the wind component observed lies along the direction bisecting the angle between the directions of the meteor from the two stations at the epoch of minimum loop range. Another difference is that the effective range is the harmonic mean of the ranges of the meteor from each station, and the wind velocity \dot{y} by equation (25) and shear a by equation (24) are to be increased by a factor $\sec(\psi/2)$, where ψ is the angle between the directions of the meteor from the two stations.

Geometrical Reduction

The geometrical reduction starts with the corrected epoch of minimum range t_0 and the corrected velocity V from each station. There remains the problem of locating for each echo an "effective station" on the bisector of the directions of the transmitter and receiver from the meteor and at the harmonic mean of the two ranges. The uncorrected epoch of minimum range and the uncorrected velocity are deduced from the epochs of the maxima and minima (extrema) of the Fresnel pattern. For a meteor of constant radar magnitude without diffusion, the relation between the epoch of minimum range and those of the extrema is derived in McKinley (1961, pp. 186-225). Southworth (unpublished) finds from numerical integrations that both the diffusion and the slope of the ionization curve have an effect in the sense that the distance x_1 from the minimum range point to the first Fresnel maximum is given by

$$x_1 = \frac{1}{2} \left[0.861 - 1.535C + 2.75C^2 - 3.0C^3 + \left(\frac{\sqrt{2}}{2} \right) CS \right] F \quad (29)$$

where F is defined as the length of the first Fresnel zone:

$$F \equiv \left(\frac{R\lambda}{1-2\alpha} \right)^{1/2} \quad (30)$$

S denotes the slope of the ionization curve in magnitudes per length F , and C is defined as

$$C \equiv \frac{8\pi D}{\lambda^2 V} \left(\frac{\lambda R}{2} \right)^{1/2} (1-2\alpha)^{-1/2} \quad (31)$$

or in terms of the time to cross the first Fresnel zone T_F ,

$$T_F \equiv \left(\frac{R\lambda}{1-2\alpha} \right)^{1/2} V^{-1} \quad (32)$$

and the decay time T_D for a drop in voltage amplitude of the signal by a factor e ,

$$T_D = \frac{\lambda^2}{16\pi^2 D} \quad (33)$$

we have

$$C = \frac{\sqrt{2}}{4\pi} \frac{T_F}{T_D} \quad (34)$$

Southworth has found that the amplitudes of the Fresnel patterns can be analyzed by smoothing out the oscillations after the first maximum and treating the smoothed curve as representing the decay of the amplitude from the principal Fresnel zone. The later oscillations then yield the amplitude of each successive Fresnel zone as it is formed. Such an analysis yields C , S , and the radar magnitude at the specular reflection point and the extrema. It also yields the distance x_1 along the trail to the first Fresnel maximum and thus the epoch of passage t_0 through minimum range. This epoch and the corrected velocity V for each radar site comprise the information for finding the radiant of the meteor. For its geometric position in the atmosphere, we require the difference in phase between the two troughs at the main site in order to place the meteor on a small circle in the sky at the epoch of minimum range.

The distance traveled between specular reflection points from one radar receiver to another is the integral of the velocity over the interval of time between the reflections. The ratio of this distance to that between the effective stations is the scalar product of the unit vector in the direction of the first site as seen from the second and the unit vector toward the radiant. The locus on the celestial sphere of all radiants satisfying this observation is a small circle about the direction of the first site as seen from the second. A second pair of sites, not nearly in the same relative direction, gives a second small circle. One of the two intersections of the circles is usually below the horizon (unless they are nearly tangent, i.e., unless the radiant is very near the horizon, a poorly determined or indeterminate case), so it can be eliminated forthwith. The remaining intersection is our desired radiant.

The specular reflection point of the meteor as seen from the main site must lie on the great circle with the radiant as its pole. Also, the difference in phase between the signals received at the two troughs yields a small circle. Again, the intersection below the horizon is eliminated. There is often an ambiguity of a few whole waves in the phase difference. Each possibility yields a different direction for the specular reflection point. These can be combined with the observed range to find heights above mean sea level. Usually, only one

value is plausible and the meteor is thus unambiguously located. If two values of height are both plausible, the meteor is rejected from further analysis.

The loop range for each receiving station is defined as the distance from the transmitter at station 3 to the meteor, plus the distance back to the receiver, plus the distance via microwave link back to station 3. This last quantity is zero at station 3, for which the loop range is merely twice the distance to the meteor. A pattern-recognition program was operated to measure the time and amplitude of each extremum of the Fresnel patterns. The spacings in the patterns are required to match from station to station. The oscillations from a smoothed curve are also found for each pattern. Next, the wind phase Φ is measured at each station at which an amplitude pattern was measured. The recorded phases from the phase detectors are in the analog form

$$s \equiv A_1 \sin \Phi \quad (35)$$

for odd pulses and

$$c \equiv A_1 \cos \Phi \quad (36)$$

for even pulses, where A_1 denotes amplitude, and Φ , the phase. Missing alternate values are interpolated.

Initially, the phases are found at the Fresnel maxima, multiples of 2π being added to preserve continuity where needed. They are then fitted by the polynomial

$$\Phi = E_0 + E_1 p + E_2 p^2 \quad (37)$$

where p is the pulse number. Next, the phase at each observed pulse after the first maximum is corrected (subscript c) for the oscillating part of the Fresnel pattern by subtraction of a rotating vector:

$$\begin{aligned} s_c &= s - C_F \sin (\phi_F + E_0 + E_1 p + E_2 p^2) \\ c_c &= c - C_F \cos (\phi_F + E_0 + E_1 p + E_2 p^2) \\ \tan \phi_c &= \frac{s_c}{c_c} \end{aligned} \quad (38)$$

Here, C_F is the amplitude of the oscillating part interpolated between extrema, and ϕ_F is the phase of the oscillating part, defined as 0 at the first extremum, π at the second, 2π at the third, etc., also interpolated. The corrected phases are fitted again with equation (37) and the process is

repeated. If E_2 is poorly determined or significantly positive, it is set arbitrarily equal to zero and a linear expression involving E_0 and E_1 alone is used instead.

The amplitude of the Fresnel pattern is next analyzed at each station with the measured range as part of the input.

The effective station positions are initially estimated at the midpoints of the straight-line segments joining them to station 3. Velocities and times are corrected by equations (27) and (28). They are then fitted to an expression of the form

$$V = B + C\bar{K} \exp(\bar{K}t) \quad (39)$$

$$\bar{K} = \frac{5}{4} \frac{\bar{V}}{H^*} \cos Z_R \quad (40)$$

where $H^* = 5.3$ km is an effective scale height, the factor $\frac{5}{4}$ is derived from experience with faint photographic meteors (it should be unity for classical nonfragmenting meteors), and the expression (39) is that found very convenient by Whipple and Jacchia (1957) for photographed meteors. Distances between specular reflection points are found by integration of equation (39), and the radiant is fitted to these and the effective stations. The specular reflection point from station 3 is found from the difference in phase at the two troughs with slight adjustment in the range from station 3 to give the best fit to all the loop ranges.

The next iteration and all successive ones begin by placing the effective stations on the bisector of the directions from the meteor to the transmitter and the receiver at a distance equal to the harmonic mean of the distances to the transmitter and the receiver. Also, the wind velocity \dot{y} by equation (25) and the shear a by equation (24) are increased by the factor $\sec(\psi/2)$, where ψ is the angle subtended by the transmitter and receiver from the specular reflection point. Iterations continue to convergence or failure.

TELEVISION EQUIPMENT AND REDUCTION OF COMBINED OPTICAL AND RADAR DATA

Image-Orthicon Television System

We have employed an image-orthicon television system loaned by the Naval Research Laboratory (NRL). It is a U.S. Navy shipboard system,

AN/SXQ-3, originally modified by G. T. Hicks and G. G. Barton of NRL to accept a lens of 105-mm focal length and 125-mm aperture. The image-orthicon tube is a General Electric 7967. The camera is fitted to a motor-driven alt-azimuth mounting. In addition, there are a control console, two helical-scan Ampex VR-7500 video tape recorders, a monitoring kinescope, and a remote 14-inch kinescope suitable for photographic recording.

The normal video format of the SXQ is 30 interlaced 875-line frames per second with separate vertical and horizontal drive signals. To facilitate magnetic tape recording of the video for our purposes, vertical and horizontal sync pulses were generated from the drive signals. We added these pulses to the video through a separate distribution amplifier. This modification made practical the use of an inexpensive helical-scan video tape recorder (Ampex VR-7500) for routine recording of observations. The recorders were slightly modified to improve the playback quality of the 875-line video by increasing the tape speed by 4 percent. Figure 2 displays a schematic arrangement of the equipment.

In order to preserve a nearly constant sensitivity independent of sky conditions, much of the automatic gain-control (AGC) circuitry was eliminated or bypassed. These modifications permitted a less frequent calibration of the sensitivity of the system.

We also modified the camera beam-current control to expand the adjustment in the very low light-level region. This enabled the image erasing beam to be carefully adjusted to erase the image-orthicon target charge slightly more slowly than the rate of deposit for images within the useful dynamic range. The resulting "image lag" not only was tolerated but in fact became a useful part of the scheme for the photometry of slower moving images.

Observing Techniques

Radar meteors are observed when the meteor is at a minimum range, i.e., when the meteor is 90° from the radiant and moving with maximum angular velocity. Optical detection systems are most sensitive for meteors near the radiant when the writing speed at the focal plane is at minimum. An optical observing site was established

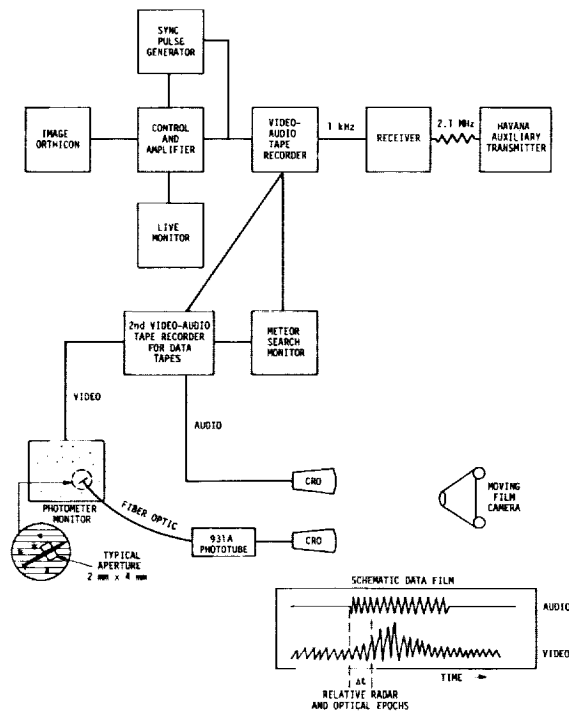


FIGURE 2.—Image-orthicon observing and data-reduction system.

near Sidell, Illinois (Long. $87^{\circ}51.2'W$, Lat. $39^{\circ}56.6'N$; $x = +185.38$ km, $y = -28.45$ km, $z = -2.67$ km). From this site, an optical system directed at elevation 49° and azimuth 263° has a maximum probability of observing objects in the meteor region at about 90-km altitude that are also observable by the Havana radar.

When operated at full sensitivity, the radar observes meteors at about 100 times the image-orthicon rate. This mismatch has two deleterious consequences. First, the problem of selecting those meteors that are true simultaneous radar and optical observations is difficult since, almost assuredly, *some* radar object will be under observation whenever the image orthicon records a meteor. Second, since the radar logic constrains the system to observing one meteor at a time, the radar data-recording system is quite likely to have been pre-empted by a faint, uninteresting meteor that occurred shortly before the brighter object was observed optically. Consequently, the radar receivers were attenuated at their input by 13 to 25 db when simultaneous observations were being attempted. To further ease the arduous task of

selecting possible simultaneous observations, the audio channel of the video tape recorded a 1000-Hz signal transmitted by an auxiliary transmitter at Havana whenever the radar data system began a record of a new meteor.

Observations were generally made during moonless skies and between 11 p.m. CST and morning twilight. Observing was usually curtailed when atmospheric extinction was variable or exceeded about 1 mag. Well-regulated line power and a 1-hour warmup ensured stability. The output was observed visually on a live monitor and recorded on tape. About 75 percent of the meteors were discovered on the live monitor, and the remaining during subsequent playbacks of the tape. Possible simultaneous observations and calibration tests were copied repeatedly on data tape for future use.

Calibration

A two-step calibration procedure was followed. A pinhole light source was set up in the loft of a nearby barn. Direct current for the source was supplied from and monitored at the image-orthicon site. The source could be attenuated remotely from the site by sequential advancement of a neutral-density step wedge located between the source and the pinhole. A total of 10 steps of 0.5-mag attenuation per step were available. These calibration observations were made with the camera slewing in altitude. Slew rates of 1° to 15° per second were used. These rates bracket the angular rates of most meteors observed simultaneously, and the fundamental calibration was thus performed on a moving source comparable to a meteor.

The second calibration step was used to define an absolute scale, in terms of stellar magnitude, for the relative response determined for the artificial light source. Stars of known brightness were recorded while the image orthicon was slewed. In general, unreddened A0 stars in or near the observing field were chosen, but on some occasions stars of spectral class as early as B8 or as late as A3 (and rarely as late as A5) were used.

In summary, the first calibration step determined what in photography is called the characteristic curve, and the second supplied the zero point for this curve in terms usually employed to define meteor luminosity. This last procedure simultaneously accounted for changes in the

image-orthicon system sensitivity and for variations in sky conditions.

Photometric Reductions

Photometry of meteors observed by photographic techniques presents problems not often encountered in astronomy or, indeed, in most areas of any science. The obvious (but seldom noted) fact that we can observe our objects only once immediately places stringent signal-to-noise restrictions on the data. The unexpected nature of the meteor event may introduce problems of dynamic range. Both problems are more serious in television techniques: System noise is much higher than for photographic emulsions, and the dynamic range is lower.

We considered two general techniques for our photometry. The first was to photograph the image-orthicon outputs—both meteor and calibration—and proceed in the manner familiar to us from our photographic work. There, we compare by eye the meteor and standard source images. We rejected this approach, however, because kinescope techniques are incapable of recording the fainter images.

The second approach was to deal directly with the electrical signal, generated from the video tape, which contains the maximum amount of undistorted information. However, observing the signal from each pixel on the meteor trail is not sufficient. It is necessary also to subtract the average signal of that pixel at a time before or after the meteor appears, i.e., to detect and account for that part of the signal that is due to night sky, stars, or system noise. Furthermore, an image orthicon does not read out its entire signal in a single frame. Since, as we learned, the integrated signal is a better and more useful measure than the peak signal is, the problem of interpreting the electrical signal is increased.

We bypassed most of these problems by physically isolating the pixels of interest on a television monitor and generating a new electrical analog signal with a phototube observing the isolated region. It might appear that this technique suffers seriously by introducing nonlinearities of the phosphor of the monitor and indeterminate effects produced by the phosphor decay. In fact, none of the effects is important so long as our calibration data are treated by the same system of analysis

as the meteor data. In a sense, we bring both the meteor and the calibration into the laboratory and observe them photoelectrically at our leisure.

In practice, all but a small area of the monitor screen—that part through which the meteor or calibration source will pass—is covered. The phototube records the luminosity of this area. The phototube output is registered on a chart recorder or displayed on a cathode-ray oscilloscope and photographed. The integrated intensity of the meteor pulse above the background is taken to be proportional to the original intensity of the source or meteor for the time interval required to pass through the aperture. It is the *integrated* intensity, rather than the peak intensity, that is pertinent since an image orthicon, and particularly one adjusted for high sensitivity, reads out the signal much more slowly than the signal is impressed on the target. We also demonstrated that the integrated intensity divided by the time the source was in the aperture was nearly independent of the angular velocity of the source, or, in terms used in photography, this system obeys the reciprocity law. (This fortunate circumstance could hardly have been anticipated since the entire photometric system contains a number of nonlinear components.) Therefore, the instantaneous intensity can be determined once the angular velocity of the meteor is known. No second-order corrections are required when the meteor and calibration source are of different angular velocities.

Photometry is performed on as many independent points on the meteor trail as is necessary to define the light curve.

Procedure for Reducing Observations of Meteors Observed by Both Radar and Television Camera

The procedure we employed in the analysis of television and simultaneous observations is one in which the position read from a plot of the meteor on a copy of a portion of a chart of the *Atlas des nördlichen gestirnten Himmels* (Schönfeld and Krüger, 1899) is combined with the radar observations to find the trajectory in the atmosphere. The zero points of the time scales for the radar and optical records as established by the start of the radar return recorded on the audio channel of

the video tape are exhibited on the light curve. The threshold for the kinescoped film is established to fit the duration on the film so that the epochs of beginning and end of the meteor as kinescoped are found. We then have positions (beginning of meteor, beginnings and ends of frames, end of meteor) at specified epochs. The reduction requires that two well-determined positions and their epochs be selected. These are often the beginning and end and will be referred to by those terms for convenience.

The linear velocity of the meteor is taken from results of the processing of the Fresnel patterns or of the complete radar reduction. Then a series of values of the range from Sidell to the end point of the meteor is introduced. A solution for the trajectory (rectangular coordinates and radiant) is found for each of these end ranges. The bisector of the directions of the transmitter and receiver from the meteor is also found for the minimum range epoch of each radar return. The cosine of the angle between this direction and the radiant is then determined. The correct solution is that at which this angle is a right angle and its cosine vanishes and is found by interpolation with respect to the end range. Errors of observation cause these values of the end range to vary from one radar station to another. An appropriate mean is adopted. Also, the loop ranges are computed from each station as a check, and the phase is computed for site 3 (the transmitter). Comparison of this phase with that measured between the two troughs at site 3 and of the computed loop ranges with their observed values serves to eliminate chance coincidences between a radar observation of one meteor and an optical observation of another. The computed loop range is usually near a minimum with respect to end range from Sidell and so cannot be used to determine that end range.

We are given at two epochs (beginning and ending) the right ascension and declination of the meteor as observed from Sidell: $t_b, \alpha_b, \delta_b; t_e, \alpha_e, \delta_e$. We are also given for each radar station n the epoch t'_n of the first Fresnel maximum, the loop range R_{3n} , and the velocity V deduced from the Fresnel pattern. We further know the alt-azimuth coordinates x_n, y_n, z_n (to the East, North, and zenith, respectively) of each station referred to site 3 as the origin, and the coordinates of Sidell

x_s, y_s, z_s . If a full radar reduction is available, the epoch of specular reflection t_n is also given.

We initially find the Greenwich Sidereal Time from the *American Ephemeris* and subtract the longitude of Havana ($+6^h0^m5.27^s$) to determine the Local Sidereal Time θ_0 . Also, we find the epochs of specular reflection t_n (if not given) at each site by application of the correction

$$\Delta t'_n = -0.4 \frac{\sqrt{\lambda(R_{3n} - R_{G3n})}}{V} \quad t_n = t'_n + \Delta t'_n \quad (41)$$

where R_{G3n} is the range of site n from site 3:

$$R_{G3n} = (x_n^2 + y_n^2 + z_n^2)^{1/2} \quad (42)$$

We commence by transforming our optical directions to hour angle and declination for the meridian of Havana as seen from Sidell:

$$t = \theta_0 - \alpha \quad (43)$$

The direction cosines on the local equatorial system are

$$\begin{aligned} \ell_E &= -\cos \delta \sin t \\ m_E &= -\cos \delta \cos t \\ n_E &= \sin \delta \end{aligned} \quad (44)$$

Here the x_E axis is directed to the east, the y_E axis to the intersection of the meridian and the equator below the horizon, and the z_E axis to the north celestial pole.

We next rotate to the alt-azimuth system of Havana:

$$\begin{aligned} \ell &= \ell_E \\ m &= m_E \sin \phi + n_E \cos \phi \\ n &= -m_E \cos \phi + n_E \sin \phi \end{aligned} \quad (45)$$

At Havana, the latitude $\phi = +40^\circ 15'$, $\sin \phi = +0.6457$, and $\cos \phi = +0.7636$. These directions are from Sidell at

$$\begin{aligned} x_s &= +185.38 \text{ km} \\ y_s &= -28.45 \text{ km} \\ z_s &= -2.67 \text{ km} \end{aligned}$$

We choose as an independent variable the range R_e at the end point of the meteor from Sidell. For

such a chosen value, the end point lies at

$$\begin{aligned} x_{me} &= R_e \ell_e + x_s \\ y_{me} &= R_e m_e + y_s \\ z_{me} &= R_e n_e + z_s \end{aligned} \quad (46)$$

Next we require the various angles in the triangle formed by Sidell and the meteor. The pole of the trail is given by

$$\begin{aligned} \ell_p \sin \alpha_{be} &= m_b n_e - m_e n_b \\ m_p \sin \alpha_{be} &= \ell_e n_b - \ell_b n_e \\ n_p \sin \alpha_{be} &= \ell_b m_e - \ell_e m_b \end{aligned} \quad (47)$$

where α_{be} is the angular distance from the beginning to the end. Then we have, by application of the law of sines,

$$\sin \theta_b = \frac{R_e}{V(t_e - t_b)} \sin \alpha_{be} \quad (48)$$

$$\theta_e = \theta_b + \alpha_{be} \quad (49)$$

Here we can use either solution of equation (48), i.e., $0 \leq \theta_b \leq 90^\circ$ or $90^\circ \leq \theta_b \leq 180^\circ$. In either case,

$$R_b = V(t_e - t_b) \frac{\sin \theta_e}{\sin \alpha_{be}} \quad (50)$$

The beginning of the meteor then lies at

$$\begin{aligned} x_{mb} &= R_b \ell_b + x_s \\ y_{mb} &= R_b m_b + y_s \\ z_{mb} &= R_b n_b + z_s \end{aligned} \quad (51)$$

The radiant has the direction cosines

$$\begin{aligned} \ell_R &= \frac{x_{mb} - x_{me}}{V(t_e - t_b)} \\ m_R &= \frac{y_{mb} - y_{me}}{V(t_e - t_b)} \\ n_R &= \frac{z_{mb} - z_{me}}{V(t_e - t_b)} \end{aligned} \quad (52)$$

At the epochs of specular reflection t_n , the meteor was at

$$\begin{aligned} x_{mn} &= x_{me} \frac{t_n - t_b}{t_e - t_b} + x_{mb} \frac{t_e - t_n}{t_e - t_b} \\ y_{mn} &= y_{me} \frac{t_n - t_b}{t_e - t_b} + y_{mb} \frac{t_e - t_n}{t_e - t_b} \end{aligned} \quad (53)$$

$$z_{mn} = z_{me} \frac{t_n - t_b}{t_e - t_b} + z_{mb} \frac{t_e - t_n}{t_e - t_b}$$

The loop range from sites 3 and n is given by

$$\begin{aligned} R_{3n} &= R_3 + R_n + R_{G3n} \\ R_n &= [(x_{mn} - x_n)^2 + (y_{mn} - y_n)^2 + (z_{mn} - z_n)^2]^{1/2} \\ R_3 &= (x_{m3}^2 + y_{m3}^2 + z_{m3}^2)^{1/2} \end{aligned} \quad (54)$$

Finally, we wish to determine how close the meteor was to minimum loop range. This can be done by formation of the derivative

$$\begin{aligned} \frac{dR_{3n}}{dt} &= \frac{dR_3}{dt} + \frac{dR_n}{dt} \\ \frac{dR_n}{dt} &= \frac{(x_{mn} - x_n)(dx/dt)}{R_n} \\ &+ \frac{(y_{mn} - y_n)(dy/dt)}{R_n} + \frac{(z_{mn} - z_n)(dz/dt)}{R_n} \end{aligned}$$

The derivatives are

$$\frac{dx}{dt} = -V\ell_R$$

$$\frac{dy}{dt} = -Vm_R$$

$$\frac{dz}{dt} = -Vn_R$$

Then we have

$$\frac{dR_n}{dt} = -\frac{V}{R_n} [(x_{mn} - x_n)\ell_R + (y_{mn} - y_n)m_R + (z_{mn} - z_n)n_R]$$

$$\begin{aligned} \frac{dR_{3n}}{dt} &= -\frac{V}{R_3 R_n} \{R_n(x_{m3}\ell_R + y_{m3}m_R + z_{m3}n_R) \\ &+ R_3[(x_{mn} - x_n)\ell_R + (y_{mn} - y_n)m_R \\ &+ (z_{mn} - z_n)n_R]\} \end{aligned} \quad (55)$$

$$\frac{dR_{33}}{dt} = -\frac{2V}{R_3} (x_{m3}\ell_R + y_{m3}m_R + z_{m3}n_R) \quad (56)$$

To put these on a dimensionless basis, we divide by $(-2V)$:

$$\mathbf{R} \cdot \mathbf{N}_n = \frac{1}{2R_3R_n} \{R_n(x_{mn}\ell_R + y_{mn}m_R + z_{mn}n_R) + R_3[(x_{mn} - x_n)\ell_R + (y_{mn} - y_n)m_R + (z_{mn} - z_n)n_R]\} \quad (57)$$

$$\mathbf{R} \cdot \mathbf{N}_3 = \frac{1}{R_3} (x_{m3}\ell_R + y_{m3}m_R + z_{m3}n_R) \quad (58)$$

Here \mathbf{R} is a unit vector toward the radiant, \mathbf{N}_n is the unit vector bisecting the directions to the meteor from sites 3 and n , and \mathbf{N}_3 is the unit vector toward the meteor from site 3.

The observation of phase gives us $\sin \phi_A$, where ϕ_A is the phase angle from the trough at site 3. The direction cosines from station 3 are

$$\begin{aligned} \ell_{33} &= \frac{x_{m3}}{R_3} = \frac{2x_{m3}}{R_{33}} \\ m_{33} &= \frac{y_{m3}}{R_3} = \frac{2y_{m3}}{R_{33}} \\ n_{33} &= \frac{z_{m3}}{R_3} = \frac{2z_{m3}}{R_{33}} \end{aligned} \quad (59)$$

and the direction cosines of the southerly perpendicular to the trough are (direction toward $A = 203^\circ$) $-\sin 23^\circ$, $-\cos 23^\circ$, 0, or -0.3907 , -0.9205 , 0.0000. The scalar product of these two unit vectors is $\sin \phi_A$:

$$\begin{aligned} \sin \phi_A &= -0.3907 \frac{x_{m3}}{R_3} - 0.9205 \frac{y_{m3}}{R_3} \\ &= -\frac{0.7814x_{m3} + 1.8410y_{m3}}{R_{33}} \end{aligned} \quad (60)$$

We repeat this process at successive ranges. We commence at $R_e = 80$ km and increase in 10-km steps to 180 km and then stop. Interpolation in R_e to fit the condition $\mathbf{R} \cdot \mathbf{N}_n = 0$ is then carried out and a suitable compromise made between the various stations in arriving at a final end range R_e . Finally, the computation is repeated at the adopted end range, and the height above mean sea level is found in the usual way from the deduced rectangular coordinates of the meteor.

The deduced ranges are used with the apparent light curve to find the light curve in absolute magnitude (standard range 100 km). The observed radar magnitude (a line density of 10^{12} per centimeter corresponds by definition to a meteor of radar magnitude +5) is then corrected for the antenna pattern established by Sekanina (1972, private communication).

Results from Simultaneous Radar and Television Observations

Twenty-nine meteors were observed and reduced simultaneously by radar and television from February 1969 through June 1970. Tables 2 to 6 list the results of these observations. The following quantities are presented in the tables:

V is the velocity of the meteor
 h_B and h_E are the beginning and end heights
 $M_{p \text{ max}}$ denotes the image-orthicon magnitude (approximately panchromatic) at maximum brightness

$$\int_{-\infty}^{+\infty} I_p dt, \quad I_p \equiv 10^{-0.4M_p}$$

is the integrated brightness (including linear extrapolations of magnitude versus time below threshold), where I_p denotes the instantaneous panchromatic brightness in units of zero absolute magnitude (reference range of 100 km)

Z_R is the zenith distance of the radiant from the zenith at Havana

Ceplecha's (1968) class with respect to beginning height is read from his figure 1
 α_R and δ_R are the right ascension and declination of the geocentric radiant (cleared of zenith attraction and diurnal aberration)

V_G is the geocentric velocity of the meteor
 M_R denotes the radar magnitude and
 M_p is the image-orthicon magnitude

The observed velocity was used for the velocity outside the atmosphere without correction for deceleration by atmospheric drag. The orbital elements are denoted by the usual symbols (semimajor axis, eccentricity, distance from the Sun at perihelion, argument of perihelion, longitude of the ascending node, inclination, and longitude of perihelion, respectively). The designations of the showers are those of Cook (1973).

TABLE 2.—Circumstances of the Observed Meteors

Meteor number	1969 UT		Radar	Optical	V (km s ⁻¹)	Radar		Optical	
						h _B (km)	h _E (km)	h _B (km)	h _E (km)
1	Feb. 14 ^d 10 ^b 57 ^m	23.50 ^a -24.48 ^a	23.76 ^a -24.13 ^a	23.50 ^a -24.48 ^a	31.2	90.6- 82.7	94.7 - 75.7		
2	Apr. 20 8 19	14.12 -14.99	14.12 -14.88	14.44 -14.99	14.7	102.1- 94.6	98.8 - 93.1		
3	July 19 7 44	6.88 - 7.86	7.13 - 7.50	6.88 - 7.86	17.1	86.4- 82.6	89.0 - 79.5		
4	July 19 8 30	6.87 - 8.16	7.81 - 8.16	6.87 - 8.16	19.8	92.5- 90.6	97.6 -(90.6)		
5	Aug. 18 7 42	53.16 -54.63	53.72 -53.95	53.16 -54.66	26.0	101.7- 96.4	110.8 -(86.0)		
6	Sept. 18 8 52	55.65 -56.48	55.65 -55.91	55.72 -56.48	20.4	97.1- 93.8	96.2 - 86.7		
7	Oct. 8 6 18	37.20 -38.86	37.42 -37.82	37.20 -38.86	17.9	94.1- 88.7	97.1 - 74.6		
8	Oct. 15 8 52	2.70 - 3.26	2.72 - 3.09	2.70 - 3.26	21.8	97.6- 92.1	97.9 -(88.6)		
9	Oct. 15 9 55	30.54 -31.08	30.66 -30.98	30.54 -31.08	28.8	104.5- 98.8	106.0 -(97.0)		
10	Oct. 22 10 44	6.03 - 7.25	6.21 - 6.59	6.03 - 7.25	32.9	98.5- 90.6	102.2 - 77.0		
11	Nov. 8 8 43	2.15 - 3.43	2.77 - 2.85	2.15 - 3.43	19.3	84.6- 83.4	94.3 - 74.4		
12	Nov. 16 7 33	7.42 - 8.25	7.42 - 7.87	7.60 - 8.25	16.2	93.4- 87.7	91.1 - 82.8		
13	Nov. 16 9 45	23.58 -24.10	23.83 -23.99	23.58 -24.10	30.2	96.7- 93.2	102.3 - 90.7		
14	Dec. 13 11 11	38.29 -38.50	38.29 -38.50	38.29 -38.50	36.0	87.7- 81.7	87.7 -(81.7)		
15	Dec. 16 9 45	46.89 -48.02	46.94 -47.24	46.89 -48.02	30.1	99.2- 92.3	100.4 - 74.4		
1970 UT									
16	Jan. 10 10 26	3.38 - 4.43	3.38 - 3.75	3.38 - 4.43	44.5	110.0-103.0	(110.0)-(91.7)		
17	Feb. 12 7 50	11.22 -12.04	11.22 -11.92	11.35 -12.04	16.9	97.8- 89.2	96.2 -(87.7)		
18	Feb. 12 9 24	24.48 -25.28	24.48 -24.74	24.66 -25.28	25.5	96.3- 92.0	93.4 - 83.4		
19	Feb. 12 10 11	44.54 -45.39	45.04 -45.39	44.54 -45.34	30.4	102.3- 95.4	112.2 ^a - 96.4		
20	Feb. 12 10 16	7.08 - 7.82	7.15 - 7.26	7.08 - 7.82	19.3	91.1- 89.6	92.0 - 82.2		
21	Feb. 12 10 36	6.12 - 6.82	6.12 - 6.45	6.14 - 6.82	32.0	95.8- 88.2	95.3 - 79.6		
22	Feb. 12 10 52	1.60 - 2.53	1.75 - 1.93	1.60 - 2.53	23.5	97.1- 93.9	99.8 - 83.3		
23	Mar. 16 10 40	58.47 -59.14	58.54 -59.10	58.47 -59.14	35.7	93.6- 83.7	94.8 - 83.2		
24	Apr. 3 9 59	43.50 -44.59	43.53 -43.72	43.50 -44.59	27.1	94.1- 89.9	94.7 - 70.0		
25	Apr. 7 7 48	48.43 -49.55	48.43 -49.22	48.61 -49.55	20.2	95.1- 84.5	92.7 - 80.1		
26	Apr. 7 9 55	20.38 -21.11	20.53 -20.75	20.38 -21.11	35.5	102.6- 96.8	106.6 - 87.2		
27	Apr. 10 8 9	11.34 -12.07	11.36 -12.07	11.34 -11.84	20.2	100.3- 91.1	100.8 -(94.1)		
28	May 5 9 19	16.73 -17.50	16.73 -17.28	16.80 -17.50	17.5	94.2- 87.0	93.3 - 84.1		
29	May 7 5 36	54.52 -56.03 ^b	54.52 -55.07	54.91 -56.03 ^b	14.7	95.7- 90.6	92.1 - 81.7 ^b		

^a Extrapolated out of field.

^b Light curve extrapolated to threshold. Ending could have been as early as 55.69^a.

Heights are referred to mean sea level. Magnitudes below threshold are indicated by an inequality sign.

Velocities are probably uncertain by a few tenths of a kilometer per second (none of these relatively bright radar meteors is a first-class example of a well-observed radar meteor); no measurable decelerations were found. Heights are uncertain by a kilometer or two, or occasionally three. The threshold absolute magnitude quoted is an average for the beginning and end of the trail if both were observed, or it refers to the beginning

alone if only it was observed and the meteor left the field while under observation. Masses are based on the suggested luminous efficiency of stone by Ayers, McCrosky, and Shao (1970).

Most of the observations appear to have been affected by fragmentation. Unmistakable evidence can be seen for this in the light curves shown in figures 3 and 4. Only the light curve of meteor no. 2 looks classical throughout. Meteors nos. 21 and 25 look classical except for an apparent exponential decay near the end, reminiscent of terminal blending. All sites received their radar

TABLE 3.—Radiant and Photometric Data for the Observed Meteors

Meteor number	M_p max	Integrated intensity, ^a $\int_{-\infty}^{+\infty} I_p dt$ (0 mag s) ^a	Cos Z_R	Cephecha's class	Threshold M_p	α_R (deg)	δ_R (deg)	V_G (km s ⁻¹)
1	+5.5	3.4×10^{-3}	0.618	B	+7.4	166	+11	29.4
2	+5.8	2.7×10^{-3} :	0.745	Above C ₁	+6.9	166	+53	10.0
3	+5.0	7.7×10^{-3}	0.612	B	+6.2	273	0	13.3
4	+3.9	—	0.273	C ₁	+5.8	299	-35	16.6
5	<<0	—	0.705	Above C ₁	+5.8	281	+54	23.7
6	+4.9	6.2×10^{-3} :	0.613	C ₁	+6.2	302	+65	17.2
7	+4.3	1.27×10^{-2}	0.751	Above C ₁	+6.7	332	+18	14.4
8	+5.6	—	0.688	C ₁	+6.1	23	+7	19.1
9	+4.9	—	0.659	Above C ₁	+5.2	30	+16	26.9
10	~0	—	0.629	C ₁	+4.9	46	+17	31.3
11	+6.1	2×10^{-3} ::	0.807	C ₁	+8.0	47	+19	16.0
12	+7.4	—	0.790	C ₁	+7.8	27	+25	12.2
13	+4.3	5.6×10^{-3} :	0.738	C ₁	+6.6	67	+18	28.4
14	+5.7	—	0.805	Below A	+7.1	120	+23	34.5
15	+6.2	—	0.778	C ₁	+7.0	94	+27	28.2
16	~-1	—	0.438	Above C ₁	+4.8	130	-9	43.3
17	+6.3	—	0.736	C ₁	+6.9	123	+12	13.1
18	+4.6	—	0.635	B	+6.6	140	+13	23.2
19	+5.2	5.4×10^{-3} :	0.652	Above C ₁	+6.4	159	+8	28.6
20	+6.3	—	0.751	B-C ₁	+7.0	137	+56	16.0
21	+6.5	2.1×10^{-3} :	0.731	B	+7.6	164	+20	30.2
22	+6.3	2.7×10^{-3} :	0.764	C ₁	+7.4	166	+25	20.9
23	+6.1	2.1×10^{-3} :	0.497	A-B	+7.2	211	-14	34.1
24	+6.3	—	0.820	B	+6.9	207	+30	25.0
25	+4.5	8.2×10^{-3} :	0.673	C ₁	+6.6	178	+5	17.2
26	+5.2	7.0×10^{-3} ::	0.744	Above C ₁	+6.2	207	+23	34.0
27	+4.1	—	0.654	Above C ₁	+6.0	187	+2	17.1
28	+5.0	6×10^{-3} :	0.764	C ₁	+5.8	214	+33	13.8
29	+5.7	6×10^{-3} :	0.640	C ₁	+6.6	111	+64	9.9

^a Uncertain integrated intensities are indicated by a colon (10 to 25 percent contribution by extrapolated parts of light curve) and very uncertain values by two colons (25 to 50 percent contribution).

returns from the classical portions of the light curves. Meteor no. 14 appears to have a classical light curve until its departure from the field of view. Meteors nos. 7, 12, 19, and 24 show strongly distorted light curves, but the early observations for each appear to have caught the meteor so soon that fragmentation had not yet degraded the radar echo. Meteors nos. 1, 9, 15, and 23 all exhibit exponential decay during the later parts of their light curves. Such a decay suggests mutual shadowing of drops against the air stream leading to mutual coalescence. This process has been discussed by Cook (1968) as an explanation for exponential decay in terminal blending. The

values of $M_R - M_p$ during the decay of light from these four meteors are so small as to suggest that this process is indeed active with a corresponding narrow spread in lines of flight of the drops. These 12 meteors appear not to have had all their radar returns weakened by fragmentations. They are no. 1 (sites 3, 4, 5), no. 2 (all sites), no. 7 (sites 4, 5), no. 9 (sites 3, 4), no. 12 (sites 3, 4), no. 14 (all sites), no. 15 (sites 4, 5), no. 19 (site 8), no. 21 (all sites), no. 23 (both sites), no. 24 (both sites), and no. 25 (all sites).

Average values were formed for $M_R - M_p$ for each meteor. Means for the two obvious groups in velocity (meteors nos. 2, 7, 12, 25 and meteors nos.

TABLE 4.—Orbits of the Observed Meteors

Meteor number	a (AU)	e	q (AU)	ω (deg)	Ω (deg)	i (deg)	π (deg)	Shower
1	1.55	0.82	0.28	306	325	7	272	Northern Virginid
2	2.31	0.57	1.00	190	30	10	220	
3	2.09	0.58	0.88	231	116	9	347	
4	1.56	0.56	0.68	85	296	8	21	
5	5.1	0.81	0.99	198	145	36	342	α Cygnid
6	1.39	0.30	0.97	212	175	30	27	
7	3.53	0.74	0.90	219	195	10	54	
8	1.60	0.64	0.58	95	22	2	116	
9	1.93	0.81	0.37	294	202	4	135	Northern Piscid
10	1.75	0.87	0.23	131	29	1	160	Southern Taurid
11	1.29	0.53	0.60	278	226	1	144	
12	1.80	0.54	0.84	236	234	4	109	
13	1.88	0.82	0.33	118	54	5	172	Southern Taurid
14	0.97	0.94	0.06	341	261	7	242	
15	2.51	0.84	0.40	288	264	4	192	Northern χ Orionid
16	56	0.99	0.31	112	110	55	221	
17	1.98	0.57	0.84	53	143	3	196	
18	3.79	0.84	0.62	79	143	2	222	Southern δ Leonid?
19	1.71	0.81	0.32	120	143	0	263	
20	2.54	0.66	0.87	225	323	16	188	
21	2.11	0.84	0.34	296	323	15	259	
22	1.20	0.60	0.47	293	323	14	256	
23	0.88	0.95	0.05	164	175	4	339	
24	3.57	0.80	0.73	247	13	27	260	
25	3.68	0.78	0.82	234	17	2	251	
26	-3.01	1.21	0.64	250	17	30	267	
27	2.49	0.69	0.78	243	20	2	263	σ Leonid
28	2.04	0.55	0.93	219	44	16	263	
29	2.10	0.53	0.99	159	46	10	205	

1, 9, 14, 15, 19, 21, 23, 24) yield a difference of higher-velocity group minus lower-velocity group of -1.0 ± 0.3 (standard deviation) mag. A linear fit with standard deviations was, therefore, found:

$$M_R - M_p = +2.85 - 3.8 (\log V - 6.408) \pm 0.16 \pm 1.3 \quad (61)$$

with the standard deviation for a single meteor being ± 0.5 mag. We note that measures consistent with this result are found over the range in height from 81.7 to 100.7 km above sea level. No measurements at all are found below these heights. This floor is presumably imposed by dissociative recombination. Meteor no. 9 was measured above this height with an underdense echo that was affected either by fragmentation or by diffusion, or by both. For meteor no. 16, the observation at 109.2 km (site 8) must have been affected by

diffusion, and all the others must have been points at which the electron trail was overdense. Estimates of the strength of the radar return that should have occurred suggest that the known uncertainty of the antenna pattern at higher altitudes has taken its toll here. Meteors nos. 5 and 25 were also vulnerable to this difficulty. These data suggest that diffusion affects measurements above a height of 101 km.

We must combine these results with the two really numerous comparisons between visual and radar meteors. The Geminids and Perseids were studied by Millman and McKinley (1956), who found a relationship between $\log T_D$ and M_V (T_D is the duration of an overdense echo in seconds, and M_V is the visual absolute magnitude). McKinley (1961, pp. 228-230) has discussed these results on the basis of Greenhow and Neufeld's (1955) relation for the coefficient of

TABLE 5.—Radar and Optical Measurements of the Observed Meteors*

Meteor number	Site	Epoch	Height (km)	M_R	M_p	$M_R - M_p$	Remarks
1	1	23.81 ^a	88.8	+ 9.7	+5.6	+4.1	Fragmentation
	2	23.91	86.9	+10.3	+5.8	+4.5	Fragmentation
	3	23.99	85.4	+ 9.3	+6.2	+3.1	Perhaps only a few fragments
	5	24.11	83.1	+ 9.5	+6.8	+2.7	
	4	24.13	82.7	+10.0	+6.8	+3.2	
2	4	14.37	99.5	+ 9.6 ^b	> +6.8	< +2.8	
	3	14.44	98.8	+ 9.4 ^b	+6.8	+2.6	
	5	14.69	96.1	+10.0	+5.8	+4.2	
3	7	14.83	94.6	+ 9.9	+5.7	+4.2	
	3	7.17	86.0	+10.4	+4.9	+5.5	All stations appear to be affected by fragmentation (see light curve)
	5	7.27	84.9	+12.1 ^b	+5.1	+7.0	
4	7.39	83.7	+12.2	+5.2	+7.0		
4	6	7.50	82.6	+13.3	+5.3	+8.0	
	3	8.04	91.3	+ 8.4	+4.1	+4.3	Strong fragmentation
5	6	8.16	90.6	+ 9.9	+4.1	+5.8	
	5	53.78	99.4	+12.1 ^b	+4.0	+8.1	
6	7	53.80	99.1	+10.9 ^b	+3.9	+7.0	
	6	53.95	96.4	+10.5	-0.5::	+11.0::	
	8	55.91	93.8	+11.2	+4.9	+6.3	Fragmentation and broad flares
7	4	37.57	92.0	+ 7.8	+5.0	+2.8	
	5	37.58	91.8	+ 8.2	+4.7	+3.5	
	6	37.82	88.7	+ 8.5	+4.4	+4.1	Fragmentation
8	1	2.78	96.7	+10.5	+6.0	+4.5	Fragmentation throughout
	2	2.86	95.6	+10.2	+5.8	+4.4	
	3	2.92	94.7	+ 9.8	+5.7	+4.1	
	4	3.09	92.1	+ 9.5	+5.7	+3.8	
9	1	30.71	103.6	+ 8.3	+5.0	+3.3	Fragmentation (rapid brightening, slow decline)
	8	30.81	101.7	+ 9.1	+4.9	+4.2	
	2	30.82	101.5	+ 8.7	+4.9	+3.8	
	3	30.90	100.0	+ 8.0	+4.9	+3.1	
	4	30.98	98.5	+ 6.5	+5.0	+1.5	
10	7	6.59	90.6	+ 9.8	+2.3:	+7.5:	Pronounced flare
11	1	2.85	83.4	+10.6	+6.8	+3.8	
12	3	7.66	90.3	+11.4	+7.8	+3.6	
	4	7.69	89.9	+10.4	+7.7	+2.7	
	5	7.87	87.7	+11.6	+7.5	+4.1	Fragmentation
13	8	23.99	93.2	+ 9.6	+5.9	+3.7	Fragmentation
14	1	38.34	86.3	+ 7.6	+6.6	+1.0	
	2	38.42	84.0	+ 8.1	+6.0	+2.1	
	3	38.50	81.7	+ 8.5	+5.8	+2.7	
15	2	47.04	96.9	+11.0	+6.5	+4.5	Light curve indicates fragmentation; last two values of $M_R - M_p$ imply relative proximity among fragments
	8	47.12	95.1	+12.0	+6.4	+5.6	
	3	47.13	94.9	+10.6	+6.4	+4.2	
	4	47.19	93.5	+ 8.6	+6.3	+2.3	
	5	47.24	92.3	+ 7.8 ^b	+6.3	+1.5	
16	8	3.43	109.2	+ 9.5 ^b	+3.5	+6.0	Undoubtedly an overdense echo undergoing rapid diffusion
	1	3.56	106.6	+ 7.9 ^b	+1.1	+6.8	
	3	3.64	105.1	+ 7.3 ^b	-0.7::	+8.0::	
	4	3.75	103.0	+ 6.4 ^b	-0.6::	+7.0::	
17	2	11.44	95.1	+10.2	+6.5	+3.7	Fragmentation
	3	11.54	93.9	+10.8	+6.3	+4.5	
	6	11.92	89.2	+10.3	+6.8	+3.5	

TABLE 5.—Radar and Optical Measurements of the Observed Meteors (Continued)

Meteor number	Site	Epoch	Height (km)	M_R	M_P	$M_R - M_P$	Remarks
18	3	24.59	94.4	+10.2	(+6.5)	(+3.7)	Large flare
	5	24.69	92.8	+13.0	(+6.4)	(+6.6)	
	4	24.74	92.0	+12.5	+6.4	+6.1	
19	8	45.12	100.7	+ 9.0	+6.2	+2.8	Fragmentation (rapid rise, slow fall)
	3	45.29	97.4	+11.6	+6.6	+5.0	
	5	45.35	96.2	+11.1	+6.6	+4.5	
20	4	45.39	95.4	+10.9	(+6.7)	(+4.2)	Fragmentation (near peak), rapid rise, slow fall
	8	7.20	90.1	+10.7	+6.4	+4.3	
	6	7.26	89.3	+11.0	+6.3	+4.7	
21	7	7.26	89.3	+10.6	+6.3	+4.3	
	2	6.15	95.1	+10.5	+7.2	+3.3	
	8	6.18	94.4	+10.5	+7.0	+3.5	
22	3	6.23	93.2	+ 9.4	+6.8	+2.6	
	4	6.31	91.4	+ 8.3	+6.6	+1.7	
	5	6.31	91.4	+ 8.9	+6.6	+2.3	
23	6	6.45	88.2	+ 9.2	+6.5	+2.7	Maximum of strongly fragmenting meteor
	2	1.81	96.0	+ 9.8	+6.2	+3.6	
	8	1.93	93.9	+11.4	+6.3	+5.1	
24	1	59.03	84.9	+ 9.0	+7.1	+1.9	Very near turning down end after slow fall; drops reconsolidated?
	5	59.10	83.7	+ 9.8	+7.2	+2.6	
25	1	43.62	92.1	+10.2	+6.5	+3.7	Echoes from stations 8, 4, 5, 6 give wild velocities, so either they are overdense (unlikely) or wind field spoils them
	2	43.72	89.9	+ 9.4	+6.5	+2.9	
26	1	48.61	92.7	+11.6 ^b	+6.4	+5.2	
	3	48.78	90.4	+ 8.8 ^b	+5.8	+3.0	
	5	48.87	89.2	+ 9.4 ^{:b}	+5.2	+4.2:	
	4	48.98	87.7	+ 8.3 ^b	+4.7	+3.6	
	6	49.22	84.5	+10.2 ^{:b}	+5.6	+4.6:	
	8	20.75	96.8	+12.7 ^{:b}	+5.3	+7.4:	
27	3	11.79	94.7	+ 8.8	+4.5	+4.3	Fragmentation
	6	12.07	91.1	+10.1	> +4.6	< +5.5	
28	1	16.78	93.6	+12.6 ^b	(+5.7)	(+6.9)	Fragmentation?
	8	17.28	87.0	+ 8.9	+5.5	+3.4	
29	4	54.63	94.6	+12.0	>> +6.4	<< +5.6	Fragmentation
	3	54.81	93.0	+10.2	> +6.4	< +3.8	
	5	55.07	90.6	+ 9.4	+5.8	+3.6	

^a Parentheses denote magnitudes extrapolated from observed light curves. Uncertain magnitudes are indicated by a colon and very uncertain values by two colons.

^b Steep gradient in antenna pattern or noise in pattern.

ambipolar diffusion of electrons and ions. He finds for the Geminids

$$M_V = 45.5 - 2.87 \log q \quad (62)$$

where q here is in electrons per meter. The definition of radar magnitude M_R is (McKinley, 1961, pp. 230-231)

$$M_R = 40 - 2.5 \log q \quad (63)$$

and thus we have

$$M_V = -0.42 + 1.148 M_R \quad (64)$$

For the Perseids, McKinley derives the expression

$$M_V = 40.0 - 2.45 \log q \quad (65)$$

TABLE 6.—Masses of the Observed Meteors*

Meteor number	Initial mass (g)	Meteor number	Initial mass (g)
1	1.0×10^{-3}	16	—
2	4.9×10^{-3} :	17	—
3	8.3×10^{-3}	18	—
4	—	19	1.8×10^{-3} :
5	—	20	—
6	5.3×10^{-3} :	21	6×10^{-4} :
7	1.43×10^{-2}	22	1.7×10^{-3} :
8	—	23	4×10^{-4} :
9	—	24	—
10	—	25	7.2×10^{-3} :
11	2×10^{-3} ::	26	1.4×10^{-3} ::
12	—	27	—
13	1.9×10^{-3} :	28	7×10^{-3} :
14	—	29	1.1×10^{-2} :
15	—		

* Uncertain mass (10 to 25 percent of total in extrapolations of light curve) is indicated by a colon; very uncertain mass (25 to 50 percent of total in extrapolations of light curve) is indicated by two colons.

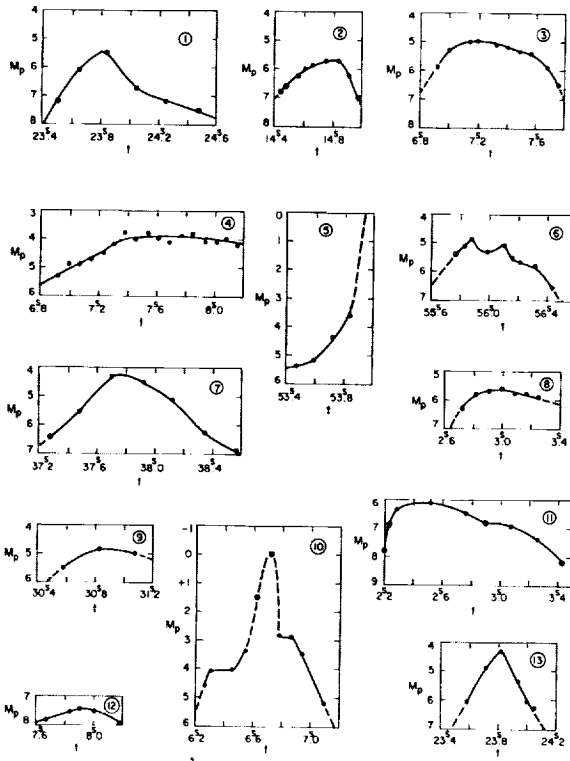


FIGURE 3.—Light curves of meteors nos. 1 to 13.

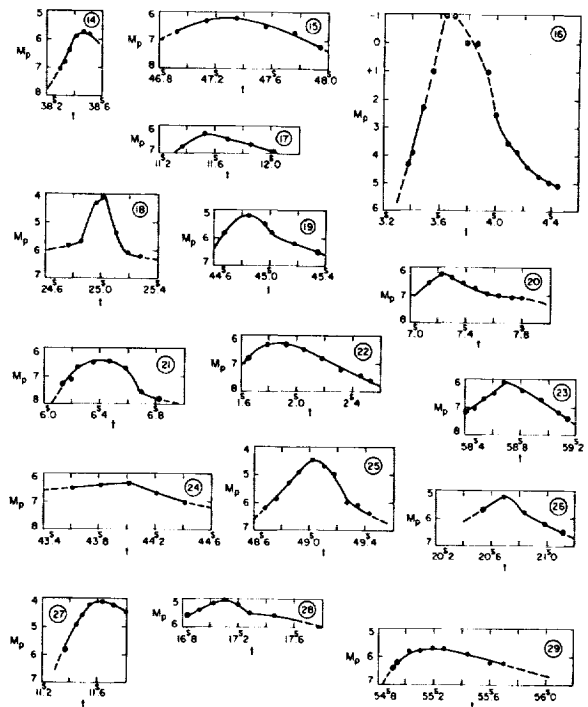


FIGURE 4.—Light curves of meteors nos. 14 to 29. Light curve of meteor no. 18 is drawn 0.6 magnitude too bright.

from which we have

$$M_V = +0.8 + 0.98M_R \quad (66)$$

The lines of regression, $\log T_D$ vs M_V and M_V vs $\log T_D$, cross at $M_V = +0.4$, $M_R = -0.4$. The deviation from unity of the coefficient of M_R for the Geminids is not significant, as it amounts to less than the unit of a half-magnitude used in quoting magnitudes even over a range of ± 3 mag from $M_V = +0.8$, $M_R = +1.0$, the crossing point of the lines of regression.

Lindblad (1963) found for the Perseids

$$\log T_D = -0.50M_V + 1.08 \quad (67)$$

where the echo duration T_D is in seconds. He also quotes

$$q = \frac{T_D}{4.5 \times 10^{-14}} \quad (68)$$

Here q is in cm^{-1} . Combination of these equations yields

$$\log q = 14.427 - 0.50M_V \quad (69)$$

$$M_R = -1.07 + 1.25M_V \quad (70)$$

Lindblad's lines of regression cross at $M_V = +1.1$, $M_R = +0.3$. We have two alternatives. In the first we accept Millman and McKinley's coefficient of M_V ; i.e., it is taken as unity. Then we have the comparisons presented in table 7.

TABLE 7.—Comparisons of Observations

Authority	log V	M_R	M_V	$M_R - M_V$
McKinley	6.556	+1.0	+0.8	+0.2
McKinley	6.781	-0.4	+0.4	-0.8
Lindblad	6.781	+0.3	+1.1	-0.8

A linear fit through these two points (the second and third points coincide) yields

$$M_R - M_V = -0.3 - 4.4(\log V - 6.668) \quad (71)$$

Our two points from the groups of radar and television meteors are given in table 8.

TABLE 8.—Data for Two Points

Point	log V	$M_R - M_p$
1	6.234	+3.5±0.2
2	6.497	+2.5±0.2

The mean of the higher of these values of log V and that for the Geminids falls at log V = 6.526. We extrapolate both fits to that value to find $M_R - M_V = +0.3$, $M_R - M_p = +2.4$. The former

value requires adjustments to panchromatic magnitudes via the color index (photographic minus visual) of -1.0 mag for faint Super-Schmidt meteors (Jacchia, 1957) and of -0.2 mag for the panchromatic index (Millman and Cook, 1959). This yields $M_R - M_p = +1.5$.

This discrepancy in $M_R - M_p$ of +0.9 mag, going from the visual observations of overdense radar meteors to the television observations of underdense radar meteors, drives us to our second alternative, which is to adopt Lindblad's coefficient of M_V . This deviates from unity by 0.25 and thus demands 3.6 mag to close the gap, leading to a fit at $M_V = +4.4$, $M_{ph} = +3.4$, $M_p = +3.2$, where M_{ph} is the photographic absolute magnitude.

A physical argument for such a behavior is that ionization should increase as we move with increasing brightness into a regime of slip flow of a meteor's own vapors.

Attention is called to the large number of light curves exhibiting a fast rise and exponential decay. This pattern suggests mutual shadowing of droplets vis-à-vis the air stream leading to mutual coalescence, a process discussed by Cook (1968) as an explanation of exponential decay in terminal blending. In this picture, no solid meteoroid is left.

ACKNOWLEDGMENTS

This work was supported in part by contract NSR 09-015-033 from the National Aeronautics and Space Administration.

REFERENCES

- AYERS, W. G., McCROSKY, R. E., AND SHAO, C. -Y., 1970. Photographic observations of 10 artificial meteors, *Smithson. Astrophys. Obs. Spec. Rept.* No. 317, 43 pp.
- CEPLECHA, ZDENĚK, 1968. Discrete levels of meteor beginning height, *Smithson. Astrophys. Obs. Spec. Rept.* No. 279, 54 pp.
- COOK, A. F., 1968. The physical theory of meteors, in *Physics and Dynamics of Meteors*, IAU Symp. No. 33, edited by Ľ. Kresák and P. M. Millman, Dordrecht, Holland, D. Reidel Publ. Co., 149-160.
- , 1972. A working list of meteor streams, this volume.
- GREENHOW, J. S., AND NEUFELD, E. L., 1955. The diffusion of ionized meteor trails in the upper atmosphere, *J. Atmos. Terr. Phys.*, **6**, 133-140.
- GROSSI, M. D., 1963. High altitude wind measurements by collecting and processing meteor radar echoes, *Record of Conference on Direct Aeronomic Measurements in the Lower Ionosphere*, Univ. of Ill., Urbana, 82-88.
- JACCHIA, L. G., 1957. On the color index of meteors, *Astron. J.*, **62**, 358-362.
- LINDBLAD, B. A., 1963. The relation between visual magnitudes of meteors and the duration of radar echoes, *Smithson. Contrib. Astrophys.*, **7**, 27-39.

- McKINLEY, D. W. R., 1961. *Meteor Science and Engineering*, New York, McGraw-Hill Book Co., 309 pp.
- MILLMAN, P. M., AND COOK, A. F., 1959. Photometric analysis of a spectrogram of a very slow meteor, *Astrophys. J.*, **130**, 648-662.
- MILLMAN, P. M., AND McKINLEY, D. W. R., 1956. Meteor echo durations and visual magnitudes, *Can. J. Phys.*, **34**, 50-61.
- SCHÖNFELD, EDUARD, AND KRÜGER, ADALBERT, 1899. *Atlas des nördlichen gestirnten Himmels*, second edition, edited and corrected by Friedrich Küstner, Bonn, Marcus und Weber.
- WHIPPLE, F. L., AND JACCHIA, L. G., 1957. Reduction methods for photographic meteor trails, *Smithson. Contrib. Astrophys.*, **1**, 183-206.